Published in Physical Review B 74, issue 155114, 1-7, 2006
which should be used for any reference to this work

Lattice-distortion-enhanced electron-phonon coupling and Fermi surface nesting in 1*T*-TaS_2

F. Clerc,* C. Battaglia, M. Bovet, L. Despont, C. Monney, H. Cercellier, M. G. Garnier, and P. Aebi
Institut de Physique, Université de Neuchâtel, Rue A.-L. Breguet 1, CH-2000 Neuchâtel, Switzerland
H. Berger and L. Forró
Institut de Physique de la Matière Complexe, EPFL, CH-1015 Lausanne, Switzerland

The temperature dependence of the electronic structure of the quasi-two-dimensional material 1*T*-TaS_2 is revisited by considering angle-resolved photoemission spectroscopy (ARPES) and density functional theory to calculate the imaginary part of the static electronic susceptibility characterizing the nesting strength. While nesting appears to play a role in the high temperature phase, the ARPES line shapes reveal peculiar spectral properties which are not consistent with the standard two-dimensional Peierls scenario for the formation of a charge density wave. The temperature dependence of these anomalous spectral features suggests a lattice-distortion enhanced electron-phonon interaction.

I. INTRODUCTION

The interplay between lattice and electronic degrees of freedom has received renewed interest in the context of high-temperature superconductivity and colossal magnetoresistance materials where electron-phonon coupling and possible polaronic effects are considered.[1,2] A significant contribution to the discussion is given by angle-resolved photoemission experiments via analysis of the spectral function. In this context it is important to examine other, more conventional materials with respect to unconventional spectral features.

1*T*-TaS_2 is a layered transition metal dichalcogenide (TMDC) with a quasi-two-dimensional character. Reduced dimensionality leads to peculiar electronic properties and an interesting phase diagram.[3] In particular, a charge density wave (CDW) occurs with three distinct phases as the temperature is lowered. It is incommensurate (IC phase) between 600 and 350 K and commensurate (C phase) with a $(\sqrt{13} \times \sqrt{13})$ periodicity below 180 K, resulting in a rotation of 13.9° with respect to the underlying unreconstructed (1×1) lattice. Between 350 and 180 K, a hexagonal array of commensurate domains with typical size of 70 Å, the so-called quasicommensurate (QC) phase, is formed. The domains are separated by domain walls, or discommensurations, where the CDW changes quickly.[4] Moreover, the transition to the C phase at 180 K is accompanied by a jump of the resistivity of more than one order of magnitude.

In one dimension (1D) the occurrence of a CDW is well explained by the theory of the Peierls instability[5,6] where a metal becomes unstable with respect to a spatially modulated perturbation with wave vector $\vec{q}_{\mathrm{CDW}}$ equal to two times the Fermi vector $2\vec{k}_F$. This leads to the formation of electron-hole pairs with the same wave vector and finally to the opening of a gap which provides a gain in electronic energy in order to compensate the elastic energy paid for the lattice distortion. The driving force for such an instability is given by the topology of the Fermi surface (FS) which has to present favorable nesting conditions. Namely, large portions of the FS have to be connected or nested by the vector $\vec{q}_{\mathrm{CDW}}$. A good indicator of the quality of the nesting is the imaginary part of the static electronic susceptibility $\chi(\vec{q})$ which, in linear response theory, relates the response of the system to the perturbation.

The Peierls mechanism is also commonly evoked in order to explain the CDW in 1*T*-TaS_2.[3,7,8] The topology of the FS of 1*T*-TaS_2 with parallel sections spanned by a vector of approximately $\vec{q}_{\mathrm{CDW}}$ has contributed to the strength of this assumption. In a recent paper,[9] it was shown that in order to confirm this scenario, the knowledge of the gap-momentum dependence is of central importance. Pillo *et al.*,[10] in their FS measurements, have observed a pseudogap over the whole FS in the C phase at a temperature below 180 K as well as in the QC phase at room temperature. The removal of states at the Fermi level (E_F) is explained by a Mott localization (electron localization of a collective nature),[11,12] which also gives rise to the strong resistivity enhancement between the QC to C phase transition. Pillo *et al.* interpreted the pseudogap observed at room temperature as a possible precursor effect of the Mott transition. Another explanation for the pseudogap is based on the spectral weight change induced by the new periodicity due to the CDW lattice distortion.[13]

These interpretations of the pseudogap are either based on electron-electron correlations or on one-electron band theory, neglecting possible effects of strong electron-phonon interaction in this CDW material where electron phonon interaction necessarily has to play an important role. The only contribution of electron-phonon interaction considered until now is the one allowing momentum transfer between electrons and holes near E_F.

Therefore it is the aim of this paper to examine the influence of electron-phonon interaction. Indeed, as nested areas of the FS can be removed by the formation of electron hole pairs during the Peierls transition, non-nested FS may also be gapped by the influence of strong enough electron-phonon coupling.[14] Moreover, the elastic energy paid for the Peierls distortion being inversely proportional to the electron-phonon coupling parameter g; strong electron-phonon interaction can help a 2D Peierls transition. In a CDW material, the electron-lattice interaction leads to a static distortion of

the whole lattice structure, but may also induce a local dynamic distortion of the lattice around the electron, forming a quasiparticle (QP) called polaron. In the case of short-range interaction it is called a small polaron, as first introduced by Holstein[15] for the study of molecular crystals. Recently, intensive numerical works have been performed on the Holstein model leading to very interesting results, notably a calculated spectral function showing a tendency towards an insulating state,[14,16,17] depending on the electronic filling or the strength of the coupling parameter g.

After describing the experimental and computational details in the next section, we will show angle-resolved photoelectron spectroscopy (ARPES) measurements for the three phases (IC, QC, and C phase). The observed spectral changes are discussed with special attention given to the influence of strong electron-phonon coupling. Low energy electron diffraction (LEED) experiments are presented to illustrate the structural changes induced by the CDW formation, and one-electron calculations based on density functional theory (DFT) are used to examine the amplitude of Fermi surface nesting. It appears that the electron-phonon coupling changes across the different CDW phases, indicating an enhancement of the coupling induced by the lattice distortion.

II. EXPERIMENTAL AND COMPUTATIONAL DETAILS

ARPES energy distribution curves (EDC's) were acquired with a Scienta SES-200 hemispherical analyzer with energy and angular resolution of ΔE=5 meV and 0.25°, respectively, while the Fermi surface mapping (FSM) measurements have been collected in a modified Vacuum Generator ESCALAB Mark II spectrometer with energy and angular resolution of 50 meV and 0.5°, respectively. The sequential motorized sample rotation has been described elsewhere.[18] Monochromatized photons of energy 21.22 eV were used for all measurements reported here.[19] 1T-TaS_2 samples were prepared by vapor transport[20,21] and cleaved *in situ* at pressures in the 10^{-11} mbar region. Surface cleanliness before and after ARPES measurements was monitored by x-ray photoelectron spectroscopy (XPS), while we used LEED to check the sample orientation and the evolution of the CDW superstructure. The Fermi energy and instrumental energy resolution were calibrated by measuring a polycrystalline copper sample. Computation of the imaginary part of the static electronic susceptibility $\chi(\vec{q})$ has been done using a recent extension to WIEN2K[22] based on the OPTICS package.[23]

III. RESULTS AND DISCUSSION

The bulk as well as the surface Brillouin zones (BZ) are shown in Fig. 1(a). In Fig. 1(b) the Ta plane is represented with arrows indicating the CDW-induced displacements that lead to the commensurate ($\sqrt{13}\times\sqrt{13}$)-R 13.9° superlattice observed in the C phase as well as in the domains of the QC phase. The displaced Ta atoms build the so-called "Star-of-David" arrangement constituted of two outer shells of six atoms and a single atom in the center of the star (this latter being the localization site in the model of Fazekas and Tosatti[11,12] that explains the Mott transition in this material). The CDW manifests itself also along the third dimension as shown by an x-ray diffraction study.[24,25]

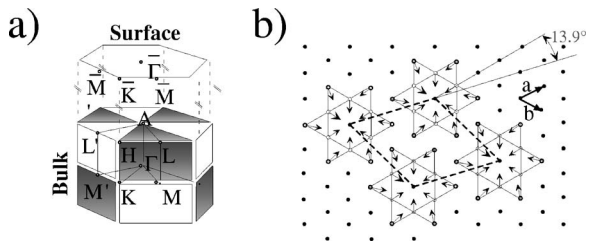

FIG. 1. (a) Surface and bulk Brillouin zones of the 1 T structure. (b) The (1×1) Ta plane. The arrows show the lattice distortions on the Ta sites shaping the "Stars-of-David" caused by the ($\sqrt{13}\times\sqrt{13}$)-R 13.9° superstructure in the commensurate CDW phase.

The LEED measurements allow one to follow the evolution of the CDW as a function of temperature. In the IC phase [Figs. 2(a) and 2(b)] one can observe the high intensity spots of the (1×1) lattice, each of them being surrounded by six less intense CDW satellite spots. Only the six superspots closest to the main spot are visible due to incommensuration.[26] In accordance with previous work[27] the superspots are aligned along the $\bar{\Gamma}\bar{M}$ direction of the (1×1) structure. Note that this is 13.9° off with respect to the CDW wave vector of the C phase. By passing through the IC to QC transition the diffraction pattern [Fig. 2(c)] shows a drastic rotation of $\sim11^{\circ}$ of the CDW satellite reflections with respect to the $\bar{\Gamma}\bar{M}$ direction. In Fig. 2(d) the orientation of the CDW spots is reported as a function of temperature. In

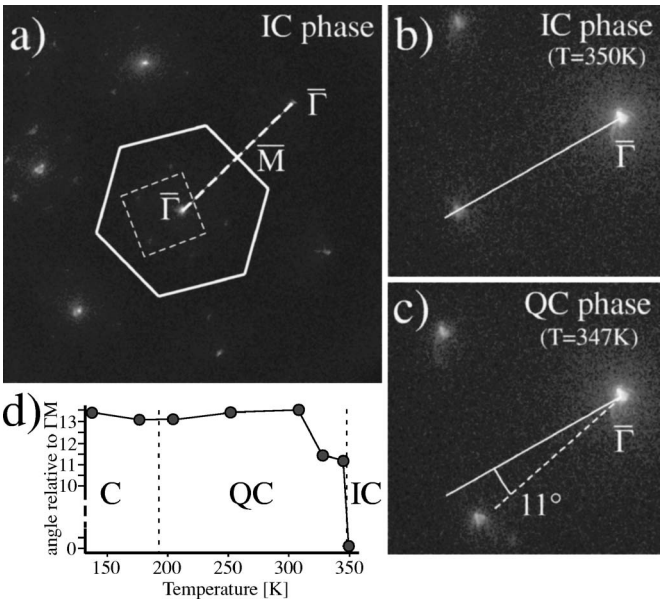

FIG. 2. Low-energy electron diffraction patterns (electron energy 93.7 eV) for (a) and (b) the IC phase and (c) the QC phase. On (a) the (1×1) hexagonal BZ is plotted and the dashed line indicates the $\bar{\Gamma}\bar{M}$ direction. (b) and (c) are zoomed pictures of the region delimited by the dashed square of (a). The lines are guide to the eye and refer to the $\bar{\Gamma}\bar{M}$ direction. (d) Temperature dependence of the angle between $\bar{\Gamma}\bar{M}$ direction and $\bar{\Gamma}$-superspot position.

good agreement with previous electron diffraction[28] and STM (Ref. 29) measurements, it appears that after a first step of $\sim 11^{\circ}$ the CDW angle is gradually increasing.

The transition from the IC phase to the QC phase has been studied theoretically on the basis of the Landau theory by McMillan[30] and more specifically for $1T$-TaS_2 by Nakanishi and Shiba.[4] Depending on the CDW-lattice interaction they predict for the QC phase a discommensuration model consisting of domains with a commensurate structure as in the C phase separated by discommensuration regions. This model has found large support thanks to STM works[31,32] and confirmation by x-ray crystal structure refinement.[25] Therefore, the rotation of $\sim 11^{\circ}$ is attributed to the appearance of domains. Although inside the domains the local angle between the CDW and the lattice is 13.9°, a slightly lower angle is measured. This discrepancy is explained by Wu *et al.*,[31] showing that the measured angle is consistent with an average CDW vector (due to different phases of the CDW in the different commensurate domains). The evolution of this angle while lowering the temperature appears to be related to the growth of the domain sizes, with the commensurate domain areas gaining weight. In our data the angle appears to go quicker to the equilibrium value than in previous experiments.[28,31] We attribute this difference to different sample quality. Indeed, a strong influence of defects on the domain sizes has been shown by Zwick.[33]

An indication of the role of electronically driven instabilities as the origin of the observed CDW in the IC phase may be provided by an estimate of the imaginary part of the static electronic susceptibility $\chi(\vec{q})$ which is defined as $\mathrm{Im}\,\chi(\vec{q}) = \Sigma_{n',n,\vec{k}} \delta(\varepsilon_{n',\vec{k}+\vec{q}} - \varepsilon_{n,\vec{k}})$, neglecting matrix elements.[34,35] The Dirac function δ gives a contribution or not depending on whether $\vec{q}$ is a nesting vector or not. Computation of $\mathrm{Im}\,\chi(\vec{q})$ is presented for two different $q_\perp$ values on linear gray scale plots in Fig. 3(a) with the white color indicating a large response of the electron system, together with $\mathrm{Im}\,\chi$ plotted along the ΓM direction. The strong intensity around $q_\parallel = 0$ is due to intraband contributions from a weakly dispersing band and is irrelevant for the nesting. Indeed, for $q_\perp = 0$, a local maximum is found around $q_\parallel = 1/\sqrt{13} \times \vec{a}^*$, consistent with Myron's[36] calculations obtained for a more limited set of $\vec{q}$ vectors. Out of the basal plane, one observes at $q_\perp = 1/13 \times \vec{c}^*$ and $q_\parallel = 1/\sqrt{13} \times \vec{a}^*$ a more pronounced local maximum confirming the out-of-plane component of the nesting vector.[24,25] Therefore, for the IC phase where the CDW is directed along ΓM and the calculated susceptibility has a distinct maximum for $q_\parallel = 1/\sqrt{13} \times \vec{a}^*$, FS nesting is a plausible explanation for the onset of the CDW. Additional confidence for a standard Peierls scenario to explain the occurrence of the ICCDW comes from Fig. 3(b) where a Fermi surface mapping (FSM) of the $1T$-TaS_2 measured at room temp erature is reproduced. We superimpose on this FSM the BZ corresponding to the IC superstructure. It clearly shows that some of the BZ boundaries of the IC superstructure follow the nested areas of the FS as expected in the standard Peierls scenario. Therefore, this result leads to a signifiant potential for electronic energy gain. But, as pointed out by Johannes *et al.*,[37] the definitive evidence of the nesting contribution to the CDW formation needs confirmation by calculation of the real part of the static electronic susceptibility. Presently this calculation is beyond our capabilities. Nevertheless, we can expect a local maximum in the real part. In fact, given the geometry of the FS of $1T$-TaS_2, the maximum in the imaginary part of the susceptibility at the correct $\vec{q}_{\mathrm{ICCDW}}$ vector can be attributed to the presence of flat areas on the FS and numerical simulation (not using DFT) for a 2D toy model (not shown), i.e., closed FS with flat areas, leads to a local maximum not only in the imaginary part of the susceptibility but also in the real part of the susceptibility.

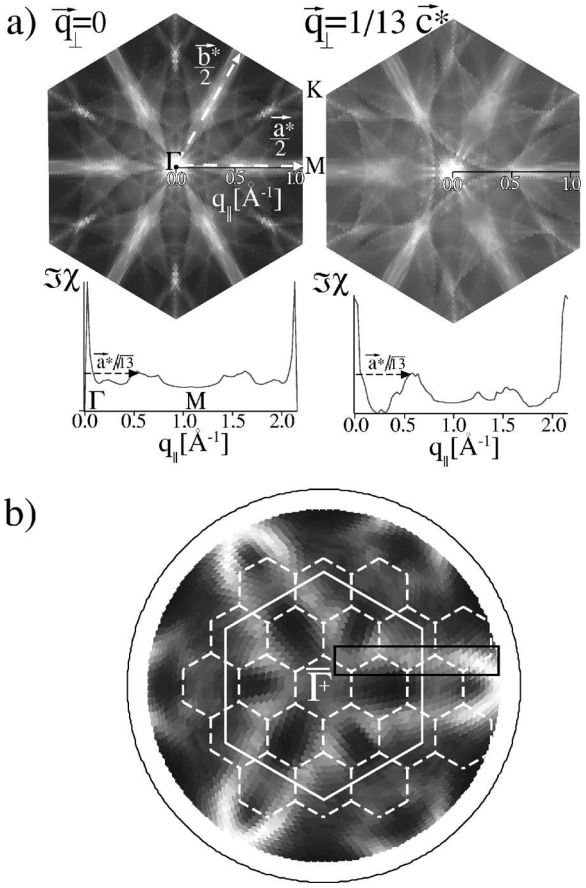

FIG. 3. (a) Top: imaginary part of the static electronic susceptibility in the first Brillouin zone at $q_\perp = 0$ (ΓMK plane) and $\frac{1}{13}c^*$. Bottom: imaginary part of the static electronic susceptibility vs momentum vector along ΓM direction. The dashed arrows correspond to the CDW vector of the IC phase extracted from diffraction measurements. (b) Fermi surface mapping measured at room temperature with the unreconstructed hexagonal BZ (white plain line) and the hexagonal BZ of the IC superstructure (white dashed line). The black rectangle is used to highlight the superposition of the nested FS areas with the BZ boundaries of the IC phase.

Figure 4 presents ARPES measurements in the IC and QC phases, taken at 350 and 344 K, respectively. The intensity plots (high intensity in black) on Fig. 4(a) are azimuthal cuts taken at a polar angle of 14° with respect to $\bar{\Gamma}$. The only visible band, near E_F, originates from Ta $5d$ electrons. In Fig. 4(b) these intensity plots are symmetrized with respect to the Fermi level and summed in order[38,39] to remove the perturbative effect of the Fermi-Dirac distribution cutoff and to infer whether the spectral function peak crosses the chemical

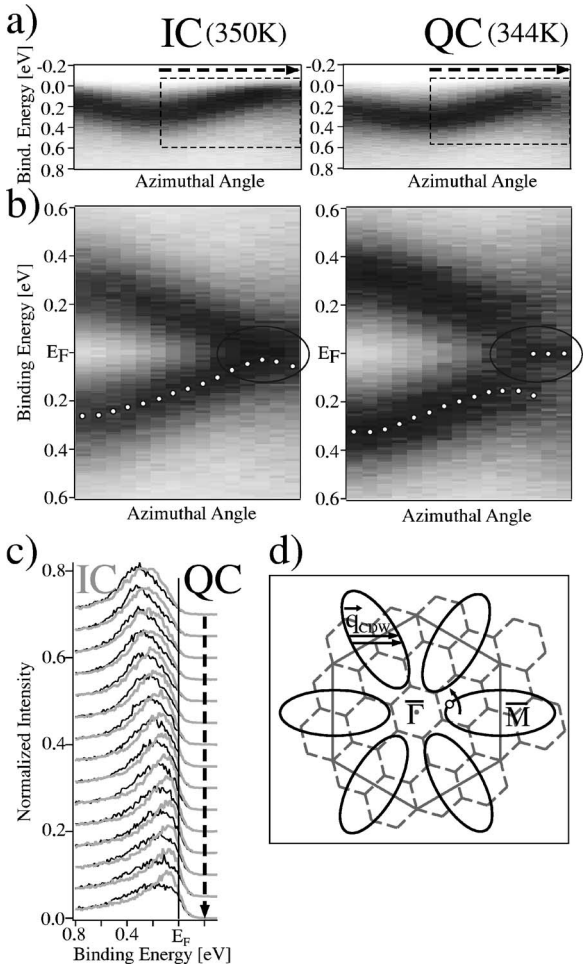

FIG. 4. (a) ARPES intensity maps measured along the azimuthal angle at a polar angle of 14° for the IC and QC phases. (b) Symmetrized plots of the zone delimited by the dashed rectangle on the maps on top. The corresponding location in the surface reciprocal space is shown by the curved arrow on the FS sketch in (d). (c) EDCs extracted from the maps plotted in (a), in black for the QC phase and gray for the IC phase. The dashed arrow is located at the same position as the dashed arrows of (a). (d) The black ellipses represent a sketch of the FS where also are superimposed the (1 $\times$1) BZ and the ($\sqrt{13}\times\sqrt{13}$)-*R* 13.9° BZ boundaries in continuous gray lines and dashed gray lines, respectively. The small white circle indicates the location where the EDCs of Fig. 5 are measured.

potential or not. Figure 4(c) shows the energy distribution curves (EDCs) corresponding to the intensity plots shown in Fig. 4(a). In Fig. 4(d) a sketch of the FS contours is drawn, together with a superposition of the normal- and commensurate-state BZs. The curved arrow indicates the location of the intensity plots of Fig. 4(a). The presumed nesting vector $\vec{q}_{\mathrm{CDW}}$ is also drawn according to the calculation of Im $\chi(\vec{q})$, connecting flat parts of the elliptically shaped FS with large, possibly nested (parallel) portions which have strongly turned the discussion of the origin of the CDW towards the nesting scenario.

As mentioned in the Introduction a clear picture of the gap momentum dependence is crucial for the interpretation of the origin of the CDW. Pillo *et al.*[10] first, and Bovet *et al.*[13] later, have both observed an entirely pseudogapped FS at room temperature (QC phase) without any differentiation between presumed nested areas, new BZ boundaries, and other FS parts. The pseudogap was either interpreted as a precursor effect of the Mott transition in the commensurate domains due to the already formed "Star-of-David" superstructure with electron localization sites at the center[10] or as a band structure effect due to the new symmetry induced by the lattice deformation.[13] Here we want to introduce a new possible explanation based on the detailed spectral features of Fig. 4. However, one has to be aware that the new interpretation does not contradict the previous ones, but gives a new point of view. As long as quantitative modeling of ARPES for realistic microscopic models is not available it is not clear to what degree a given interpretation is unique.

Consistently with the two previous authors we have performed the same measurements on large parts of the FS (not shown) and we do not observe a different behavior than that shown in Fig. 4 and described in the following. In the IC phase [Fig. 4(a) and 4(b), left] a broad Ta 5*d* band flattens and narrows slightly when approaching E_F, giving rise to a small maximum centered at E_F in the symmetrized plot. In a standard interpretation of the symmetrization procedure this would be attributed to a Fermi level crossing of the quasiparticle peak (QP). However, band calculations predict a linear slope through E_F and no flattening as observed. Moreover, within the Fermi-liquid picture ARPES peaks are attributed to QP excitations whose lifetime increases when approaching E_F. However, in our case the Ta 5*d* peak remains anomalously broad near E_F. Thus we are clearly in the presence of a renormalized band which touches E_F without clearly crossing it. Also, a renormalization of the entire FS, as observed, is not consistent with an explanation based solely on a 2D Peierls scenario. Since the interaction of electrons with the lattice is a key aspect of the CDW instability, a natural candidate to explain these anomalous spectral properties is electron-phonon coupling which can induce polaronic effects.[1,40,41] A polaron is the fermionic QP made of an electron surrounded by a local lattice distortion which enhances its mass. Depending on the strength and the character of the interaction, the spectral changes induced by the electron-phonon coupling can be more or less dramatic. But, in any case, they are reflected by a band flattening and a partial or complete transfer of the spectral weight from the coherent QP to a broad incoherent part on the high binding energy side (for a detailed view of changes induced in the spectral function, see Refs. 1, 14, and 40–42). A polaronic scenario could thus explain the apparent absence of QP crossing as well as the broad line shape and the isotropically pseudogapped experimental FS.

An enhancement of the previous anomalies can be observed upon cooling down to the QC phase [Fig. 4(c)]. The line shape gets abruptly broader (when lowering T by only 6 K), the center of mass of the Ta 5*d* band shifts towards higher binding energy when approaching the Fermi vector and becomes clearly separated from a small maximum visible in the symmetrized plot [Fig. 4(b), right]. This symmetrization peak originates from a finite spectral weight near E_F. Bovet *et al.*[13] attributed this to a reconstructed band coming from above and merely straddling E_F. In the polaronic picture proposed here, this finite intensity near E_F is also

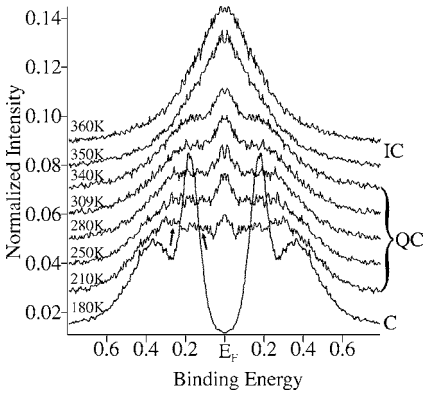

FIG. 5. Temperature dependence of symmetrized ARPES spectra. All the spectra are taken at the position indicated by the white circle on the FS sketch of Fig. 4(d). The arrows point to the two separated structures discussed in the text.

compatible with a remnant weight of the coherent QP.[14]

The changes between the photoemission spectra of the IC and QC phases are abrupt and are interpreted as a change of the electron-phonon interaction character. Indeed, in 2D or 3D systems there is a qualitative dependence of the polaron type (large or small) on the range of the electron-lattice interaction.[43] While large polarons are formed if the electron-lattice interaction due to the long range Coulombic interaction between electronic carriers and lattice ions is of predominant importance, small polarons form if the short range electron-lattice interaction such as the deformation potential interaction dominates. As shown above, the transition to the QC phase is characterized by the formation of commensurate domains composed of the so-called "Stars-of-David" clusters. These small clusters can be identified with small molecules acting as potential wells and hence favor the short range interaction. Therefore, the static deformation of the whole lattice structure induced by the CDW in the IC phase leads, in turn, to a more local character of the electron-lattice interaction and an enhancement of the electron-phonon coupling strength, i.e., to a lattice distortion enhanced electron-phonon coupling.

A complete evolution of the symmetrized EDCs as a function of temperature is represented in Fig. 5. These EDCs are all measured at the position indicated by the white circle on the FS sketch of Fig. 4(d). The abrupt changes when going from the IC to the QC phase are obvious: the broad feature centered at E_F in the IC phase is split into a small maximum and a broad hump on the higher binding energy side in the QC phase. Inside the QC phase, a smooth variation, reflected by a slightly decreasing intensity at E_F and a spreading of the hump towards higher binding energy is observed when lowering the temperature. The hump structure even splits up into two structures at binding energies of 0.125 and 0.270 eV, as indicated by the two arrows. This is in agreement with the domain size growth observed by STM,[31,32] with a continous shrinkage of the discommensurate region which hence has less weight in the ARPES intensity and thus allows the appearance of the commensurate electronic structure which is split into sub-bands.[44] Moreover, as was mentioned by Zwick *et al.*,[33] the number of free carriers able to screen electron-electron as well as electron-phonon interaction steadily decreases along with the domain growth. Therefore, the evolution of the spectral line shape in the QC phase is also influenced by a variation of the electron-lattice coupling.

The transition into the C phase (Mott transition[11,12]) introduces more drastic modifications in the symmetrized curves, with the disappearance of the small maximum at E_F and the strong intensity enhancement of the peak closest to the Fermi level accompanied by a shift of $\approx$60 meV towards higher binding energy. Moreover, the splitting of the Ta 5*d* band into sub-bands, as predicted by the Tosatti and Fazekas model, appears very clearly. All these spectral changes were previously attributed to a change of regime, with the electron-electron correlation strongly dominating the physics of the C phase, leading to a Mott transition. It is interesting to note that the splitting of the Ta 5*d* band takes place above the occurrence of the Mott transition. This splitting has the effect of strongly reducing the electronic bandwidth and, in parallel, contributing to the increase of the relative weight of the Hubbard repulsion term, confirming that favorable conditions for the Mott insulator transition are induced by the CDW reconstruction.

In Fig. 6(a) FSM measured at 20 K is plotted with respect to the wave vector component parallel to the surface. The (1×1) BZ is superimposed as well as the new BZ due to the commensurate CDW, illustrated by the small hexagons. What is reported is the photoelectron intensities (gray scale, with high intensity in white) measured in a narrow energy window around E_F, as a function of emission angle. The outer circle corresponds to grazing emission. Having identified no clear QP crossing of E_F in the previously discussed data we note that the experimental FSM is a pattern reflecting the anisotropic distribution of the remaining spectral weight of the electrons at E_F. The obtained pattern with high intensity features centered in the small hexagons is fully consistent with the $(\sqrt{13}\times\sqrt{13})$-*R* 13.9° symmetry of the commensurate superstructure. For larger polar angles the correspondence is less perfect, and the absence of intensity at the center of some hexagons may be explained by matrix element arguments used to explain the absence of branches of the elliptically shaped normal state FS.[45] In Fig. 6(b) EDCs measured along the new $\bar{\Gamma}$ points [indicated by the white dashed arrow in Fig. 6(a)] are shown in gray scale with high intensity in black. According to the "Star-of-David" picture and its inequivalent Ta atoms, one can distinguish three smoothly dispersing Ta 5*d* sub-bands, two completely filled at binding energies of 0.43 and 0.9 eV and the lower Hubbard band (LHB) closer to E_F. By zooming into the dispersion of the LHB [see Fig. 6(c)], after adjusting the gray scale, one can observe decreased spectral weights at the new BZ boundary positions (indicated by arrows) and increased spectral weights at the new $\bar{\Gamma}$ points. We therefore conclude that the intensity peaks in the FSM result from the dispersion of the LHB. In a recent article[46] the authors identify a splitting of the LHB, presumably induced by magnetic ordering with a new periodicity. However, in view of the perfect correspondence of the LHB dispersion with the CDW induced BZs, we preferably attribute these structures to the commensurate superstructure and note that the periodic depletion of spectral

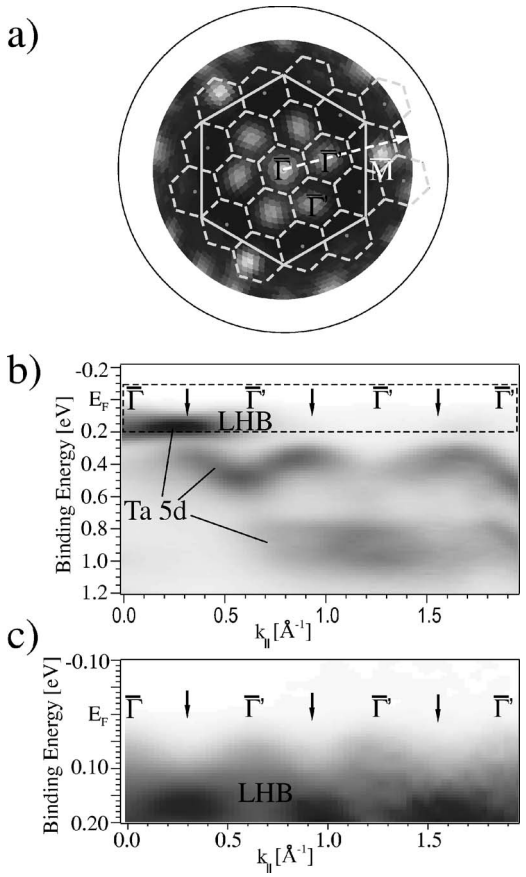

FIG. 6. (a) Fermi-surface map measured in the C phase. Superposed on it are the (1×1) BZ boundaries as well as the BZ boundaries of the commensurate superstructure in thin dashed lines. (b) ARPES intensity map measured in the direction of the new $\bar{\Gamma}$ points of the $(\sqrt{13}\times\sqrt{13})$-*R* 13.9° superstructure. The corresponding direction in surface reciprocal space is given by the dashed white arrow on the FSM. (c) Zoom and renormalization of the region delimited by the dashed rectangle in (b). The small arrows in (b) and (c) point to the location of the new BZ boundaries.

weight [arrows in Fig. 6(c)] is attributed to the CDW gap which follows the new BZ boundaries. Indeed, if we base our conclusions on the results of Sangiovanni *et al.*[47] who observed that in a strongly correlated regime where the Hubbard repulsion is the dominant scale, the electron-phonon coupling has basically no effect on the QP spectral shape anymore, we can expect that these modulations in the LHB were hidden in the QC phase by the influence of electron-phonon interaction, and reappear in the C phase when going to the strong electron-electron correlation regime.

IV. SUMMARY AND CONCLUSION

We have investigated the temperature dependence of the electronic structure of $1T$-TaS_2. The computation of the imaginary part of the static susceptibility reveals a small and broad local maximum at a q value in good agreement with the expected nesting vector for the IC phase. Additionally the superposition on the FSM of the BZ corresponding to the IC superstructure shows the possibility of a significant potential of electronic energy gain. These two observations point strongly towards the Peierls mechanism to explain the IC-CDW phase occurence. We exploited ARPES to study the band structure in the three phases (IC-QC-C). In contradiction with a pure 2D Peierls scenario, we did not find any clear QP crossing in the QC phase as well as in the IC phase but, instead, we observed a broad dispersing feature with renormalized dispersion while approaching the Fermi level. Based on polaronic considerations, we can understand these anomalous spectral properties. However, the presence of polarons has to be confirmed by other methods. Available optical measurements do not allow us to accept or reject this point of view.[48] More precise data in the midinfrared region as a function of temperature are needed. By interpreting the "Star-of-David" cluster as a small molecule we invoke a possible interplay between long range and short range electron-lattice interaction which may well enhance the strength of the coupling and hence give even more support to the polaronic point of view. By lowering the temperature through the Mott transition, the physics changes to a strongly correlated electron-electron interaction regime. The C phase data is in perfect agreement with the symmetry of the commensurate superstructure and even reveals a dispersive modulation of the LHB which allows us to locate the CDW gap at the position of the new BZ boundaries. To conclude, it turns out that although $1T$-TaS_2 has been studied for decades, its complex phase diagram and the mechanism behind the CDW formation are still a subject of debate. As long as quantitative simulations of ARPES data with realistic microscopic models are still missing, it is not clear to what point a given interpretation is unique. Nevertheless, the qualitative agreement of the behavior of our measured line shapes with a scenario based on the presence of polarons presents a new point of view to explain instabilities in $1T$-TaS_2.

ACKNOWLEDGMENTS

We are grateful to Claudia Ambrosch-Draxl for extending the optic package of WIEN2K to the computation of susceptibility. Skillful technical assistance was provided by our workshop and electric engineering team. This project has been supported by the Fonds National Suisse pour la Recherche Scientifique.

*URL: http://www.unine.ch/phys/; Electronic address: florian.clerc@unine.ch

[1] D. S. Dessau, T. Saitoh, C.-H. Park, Z.-X. Shen, P. Villella, N. Hamada, Y. Moritomo, and Y. Tokura, J. Supercond. **12**, 273 (1999).
[2] A. Lanzara, P. V. Bogdanov, X. J. Zhou, S. A. Kellar, D. L. Feng, E. D. Lu, T. Yoshida, H. Eisaki, A. Fujimori, K. Koshio, J.-I. Shimoyama, T. Noda, S. Uchida, Z. Hussain, and Z.-X. Shen, Nature (London) **412**, 510 (2001).
[3] J. A. Wilson, F. J. Di Salvo, and J. Mahajan, Adv. Phys. **24**, 117 (1975).
[4] K. Nakanishi and H. Shiba, J. Phys. Soc. Jpn. **53**, 1103 (1984).
[5] R. E. Peierls, *Quantum Theory of Solids* (Oxford University Press, Oxford, 1955).
[6] G. Grüner, *Density Waves in Solids* (Addison-Wesley, Reading, MA, 1994).
[7] H. W. Myron and A. J. Freeman, Phys. Rev. B **11**, 2735 (1975).
[8] A. M. Woolley and G. Wexler, J. Phys. C **10**, 2601 (1977).
[9] F. Clerc, M. Bovet, H. Berger, L. Despont, C. Koitzsch, M. G. Garnier, and P. Aebi, Physica B **351**, 245 (2004).
[10] Th. Pillo, J. Hayoz, H. Berger, M. Grioni, L. Schlapbach, and P. Aebi, Phys. Rev. Lett. **83**, 3494 (1999).
[11] P. Fazekas and E. Tosatti, Philos. Mag. B **39**, 229 (1979).
[12] P. Fazekas and E. Tosatti, Physica B **99**, 183 (1980).
[13] M. Bovet, D. Popovic, F. Clerc, C. Koitzsch, U. Probst, E. Bucher, H. Berger, D. Naumovic, and P. Aebi, Phys. Rev. B **69**, 125117 (2004).
[14] M. Hohenadler, D. Neuber, W. von der Linden, G. Wellein, J. Loos, and H. Fehske, Phys. Rev. B **71**, 245111 (2005).
[15] T. Holstein, Ann. Phys. (N.Y.) **8**, 325 (1959).
[16] S. Sykora, A. Hübsch, K. W. Becker, G. Wellein, and H. Fehske, Phys. Rev. B **71**, 045112 (2005).
[17] M. Hohenadler, M. Aichhorn, and W. von der Linden, Phys. Rev. B **68**, 184304 (2003).
[18] P. Aebi, J. Osterwalder, P. Schwaller, L. Schlapbach, M. Shimoda, T. Mochiku, and K. Kadowaki, Phys. Rev. Lett. **72**, 2757 (1994).
[19] Th. Pillo, L. Patthey, E. Boschung, J. Hayoz, P. Aebi, and L. Schlapbach, J. Electron Spectrosc. Relat. Phenom. **97**, 243 (1998).
[20] B. Dardel, M. Grioni, D. Malterre, P. Weibel, Y. Baer, and F. Lévy, Phys. Rev. B **45**, 1462 (1992).
[21] B. Dardel, M. Grioni, D. Malterre, P. Weibel, Y. Baer, and F. Lévy, Phys. Rev. B **46**, 7407 (1992).
[22] P. Blaha, K. Schwarz, G. Madsen, D. Kvasnicka, and J. Luitz, WIEN2K, *An Augmented Plane Wave + Local Orbitals Program for Calculating Crystal Properties* (Karlheinz Schwarz, Technical University, Wien, Austria, 2001), ISBN 3-9501031-1-2.
[23] C. Ambrosch-Draxl and J. O. Sofo, cond-mat/0402523 (unpublished).
[24] M. Bovet, S. van Smaalen, H. Berger, R. Gaal, L. Forro, L. Schlapbach, and P. Aebi, Phys. Rev. B **67**, 125105(R) (2003).
[25] A. Spijkerman, J. L. de Boer, A. Meetsma, G. A. Wiegers, and S. van Smaalen, Phys. Rev. B **56**, 13757 (1997).
[26] A. W. Overhauser, Phys. Rev. B **3**, 3173 (1971).
[27] C. B. Scruby, P. M. Williams, and G. S. Parry, Philos. Mag. **31**, 255 (1975).
[28] T. Ishiguro and H. Sato, Phys. Rev. B **44**, 2046 (1991).
[29] R. E. Thomson, B. Burk, A. Zettl, and J. Clarke, Phys. Rev. B **49**, 16899 (1994).
[30] W. L. McMillan, Phys. Rev. B **14**, 1496 (1976).
[31] X. L. Wu and C. M. Lieber, Phys. Rev. Lett. **64**, 1150 (1990).
[32] B. Burk, R. E. Thomson, A. Zettl, and J. Clarke, Phys. Rev. Lett. **66**, 3040 (1991).
[33] F. Zwick, H. Berger, I. Vobornik, G. Margaritondo, L. Forro, C. Beeli, M. Onellion, G. Panaccione, A. Taleb-Ibrahimi, and M. Grioni, Phys. Rev. Lett. **81**, 1058 (1998).
[34] C. Koitzsch, J. Hayoz, M. Bovet, F. Clerc, L. Despont, C. Ambrosch-Draxl, and P. Aebi, Phys. Rev. B **70**, 165114 (2004).
[35] C. Battaglia, H. Cercellier, F. Clerc, L. Despont, M. G. Garnier, C. Koitzsch, P. Aebi, H. Berger, L. Forró, and C. Ambrosch-Draxl, Phys. Rev. B **72**, 195114 (2005).
[36] H. W. Myron, J. Rath, and A. J. Freeman, Phys. Rev. B **15**, 885 (1977).
[37] M. D. Johannes, I. I. Mazin, and C. A. Howells, cond-mat/0510390 (unpublished).
[38] M. R. Norman, H. Ding, M. Randeria, J. C. Campuzano, T. Yokoya, T. Takeuchi, T. Takahashi, T. Mochiku, K. Kadowaki, P. Guptasarma, and D. G. Hinks, Nature (London) **392**, 157 (1998).
[39] J. Mesot, M. Randeria, M. R. Norman, A. Kaminski, H. M. Fretwell, J. C. Campuzano, H. Ding, T. Takeuchi, T. Sato, T. Yokoya, T. Takahashi, I. Chong, T. Terashima, M. Takano, T. Mochiku, and K. Kadowaki, Phys. Rev. B **63**, 224516 (2001).
[40] L. Perfetti, H. Berger, A. Reginelli, L. Degiorgi, H. Hochst, J. Voit, G. Margaritondo, and M. Grioni, Phys. Rev. Lett. **87**, 216404 (2001).
[41] L. Perfetti, S. Mitrovic, G. Margaritondo, M. Grioni, L. Forró, L. Degiorgi, and H. Hochst, Phys. Rev. B **66**, 075107 (2002).
[42] G. D. Mahan, *Many-Particle Physics* (Plenum, New York, 1981).
[43] D. Emin, Phys. Rev. B **48**, 13691 (1993).
[44] Th. Pillo, J. Hayoz, D. Naumovic, H. Berger, L. Perfetti, L. Gavioli, A. Taleb-Ibrahimi, L. Schlapbach, and P. Aebi, Phys. Rev. B **64**, 245105(R) (2001).
[45] N. V. Smith and M. M. Traum, Phys. Rev. B **11**, 2087 (1975).
[46] L. Perfetti, T. A. Gloor, F. Mila, H. Berger, and M. Grioni, Phys. Rev. B **71**, 153101 (2005).
[47] G. Sangiovanni, M. Capone, C. Castellani, and M. Grilli, Phys. Rev. Lett. **94**, 026401 (2005).
[48] L. V. Gasparov, K. G. Brown, A. C. Wint, D. B. Tanner, H. Berger, G. Margaritondo, R. Gaál and L. Forró, Phys. Rev. B **66**, 094301 (2002).